ADVANCED FUNCTIONAL MATERIALS
www.afm-journal.de

Tumor Intracellular-Environment Responsive Materials Shielded Nano-Complexes for Highly Efficient Light-Triggered Gene Delivery without Cargo Gene Damage

*Sin-jung Park, Wooram Park, and Kun Na**

Gene therapy has great potential to bring tremendous improvement to cancer therapy. Recently, photochemical internalization (PCI) has provided the opportunity to overcome endo-lysosomal sequestration, which is one of the main bottlenecks in both gene and chemotherapeutic delivery. Despite PCI having shown great potential in gene delivery systems, it still remains difficult to perform due to the photo-oxidation of exogenous cargo genes by reactive oxygen species (ROS) generated from activated photosensitizers (PSs). In this paper, a new type of a stable light-triggered gene delivery system is demonstrated based on endo-lysosomal pH-responsive polymeric PSs, which serve as shielding material for the polymer/gene complex. By taking advantage of the endo-lysosomal pH-sensitive de-shielding ability of the pH-responsive shielding material incorporated in the ternary gene complexes (pH-TCs), a more significant photo-triggered gene expression effect is achieved without damage to the gene from ROS. In contrast, pH-insensitive material-shielded nanocarriers cause photo-oxidation of the payload and do not generate a notable transfection efficacy. Importantly, with the benefit of our newly developed gene delivery system, the deep penetration issue can be resolved. Finally, the light-triggered gene delivery system using pH-TCs is applied to deliver the therapeutic p53 gene in melanoma K-1735 bearing mice, showing excellent therapeutic potential for cancer.

1. Introduction

Gene therapy has great potential as a promising therapeutic approach for cancer therapy.[1] To achieve efficient delivery of therapeutic genes, various nanoparticular gene delivery systems have been developed, including polymeric nanoparticles,[2] micelles,[3] and liposomes.[4] Despite the significant development of gene carriers based on nanotechnology, conventional systems have achieved rather limited success due to the biological barriers (e.g., reticuloendothelial system, extracellular matrix, extracellular membrane, and endo-lysosomal membrane) present under in vivo conditions.[5] Among them, endosomal sequestration is one of the main bottlenecks in both gene and chemotherapeutic delivery because the uptake of foreign materials usually relies on the cell's innate endocytic uptake mechanism.[6] This endocytic uptake pathway ultimately leads to the degradation of the drugs by fusion with a lysosomal compartment, which has harsh acidic and degradative lysosomal enzymes.[7] Poor tissue penetration is another significant drawback of nanoparticle-based gene delivery, which results in low therapeutic efficacy and poor biodistribution.[8] Unlike normal tissues, the microenvironment of a solid tumor is composed of an altered extracellular matrix, increased collagen content and density, and increased interstitial fluid pressure.[9] These conditions hinder drug penetration into the deep tumor tissues and led to drug resistance and chemotherapeutic treatment failure.

Photochemical internalization (PCI) has recently emerged as an attractive technique for overcoming endo-lysosomal sequestration.[10] The mechanism of light-triggered drug delivery is based on the destruction of extracellular or endo-lysosomal membranes by the reactive oxygen species (ROS) generated from activated PS. Consequently, it allows the cargo drugs to be liberated by degradation-mediated inactivation caused by the harsh acidic conditions in endo-lysosomes. In our previous study, we reported light-activated ternary complexes, which consist of a polyethyleneimine (PEI)/EGFR-shRNA complex core and PS-conjugated chondroitin sulphate, for systemic gene therapy in colon cancer.[11] In this system, the ternary complexes showed improved stability for shRNA protection under extracellular conditions, and their endo-lysosomal-rupturing ability resulted in a significant EGFR-mRNA silencing efficacy (≈80% knockdown). However, even though the ternary complex system in light-triggered gene delivery has provided an attractable solution to circumvent endo-lysosomal sequestration, ROS-mediated degradation of exogenous cargo genes carried in nanocomplexes still remains a problem because some payloads may also be photo-oxidized due to localization near the activated PSs, which generate ROS.[12]

Hence, here, we designed a new type of stable light-induced gene delivery system based on endo-lysosomal pH-responsive polymeric PS as a shielding material for the polymer/gene

Dr. S.-j. Park, Dr. W. Park, Prof. K. Na
Center for Photomedicine
Department of Biotechnology
The Catholic University of Korea
43 Jibong-ro, Wonmi-gu, Bucheon-si,
Gyeonggi-do 420-743, Korea
E-mail: kna6997@catholic.ac.kr

DOI: 10.1002/adfm.201500737

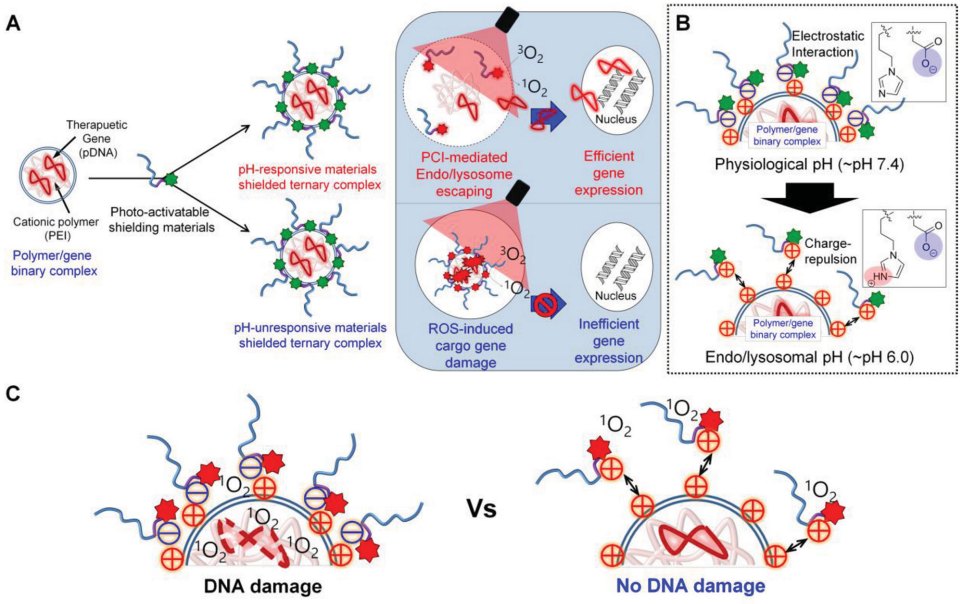

Scheme 1. Schematic representation of tumor intracellular-environment responsive materials shielded nano-complexes. A) PCI-mediated endo-lysosomal escaping in pH-responsive materials shielded ternary complexes or pH-unresponsive materials shielded ternary complexes. B) pH-dependent shielding and de-shielding behavior of pH-responsive shielding materials and chemical structural representation of the protonation of the imidazole groups in pH-responsive shielding materials at an endo-lysosomal pH. C) ROS-mediated DNA damage by conventional pH-unresponsive materials shielded ternary complexes versus protection of the cargo gene from ROS-induced nucleic acid damage by de-shielding of pH-responsive materials at endo-lysosomal pH during PCI-induced gene transfection.

complex for cancer gene therapy (**Scheme 1**). The p53 gene is an important tumor suppressor gene and plays a central role in regulating cell-cycle progression and DNA repair as well as controlling apoptosis.[13] This system is composed of a p53 gene/PEI core and a PS-conjugated pH-sensitive polypeptide that is capable of de-shielding at endo-lysosomal pH to protect the cargo gene from ROS-induced nucleic acid damage during PCI-induced gene transfection. Furthermore, we expected that the PS that broke down the extracellular matrix barrier could increase the ability of the nano-complexes to deeply penetrate into tumors. Therefore, our approach would permit us to simultaneously overcome intra/extracellular barriers without undesirable cargo gene damage.

2. Results and Discussion

2.1. Synthesis and Characterization of pH-Responsive Shielding Materials

The procedure for the synthesis of pH-responsive shielding materials is presented in **Figure 1**A. As in our previous reports,[14,15] poly(ethylene glycol)-poly(β-benzyl-L-aspartate) (mPEG-p(Bz-L-Asp)) was synthesized through the ring-opening polymerization of benzyl-L-aspartate *N*-carboxyanhydride by initiation from α-methoxy-ω-amino poly(ethylene glycol) (mPEG-NH_2). Then, pheophorbide-a (PPba)-grafted mPEG-p(Bz-L-Asp) was prepared using conventional carbodiimide coupling reagents to conjugate the carboxyl group of PPba with mPEG-p(Bz-L-Asp). To impart pH sensitivity, benzyl groups of mPEG-p(Bz-L-Asp)-PPba were substituted with 1-(3-aminopropyl) imidazole (API, pK_a, ≈6.8) by an aminolysis reaction.[16] The pH-insensitive shielding material (mPEG-p(L-Asp)-PPba, as a control, Figure S1, Supporting Information) was prepared by the deprotection of the benzyl group of the mPEG-p(Bz-L-Asp)-PPba in alkaline solution. The representative ^{1}H-NMR spectrum of pH-responsive shielding materials (i.e., mPEG-p(API-L-Asp)-PPba) is shown in Figure 1B. The benzyl peak at 7.3 ppm disappeared in the ^{1}H-NMR spectra of mPEG-p(Bz-L-Asp)-PPba and mPEG-p(L-Asp)-PPba, which indicate that phenyl ester was successfully removed. New peaks at 6.8, 7.1, and 7.6 were assigned to the protons of the imidazole ring, which demonstrated the successful substitution of the imidazole ring. The substitution ratio was calculated based on ^{1}H-NMR and GPC analysis (Figure S2, Supporting Information), and the result is summarized in Table S1 (Supporting Information).

Understanding the physicochemical properties changes of pH-responsive shielding materials at different pH values is a key factor for the intracellular pH-triggered gene delivery. The pH-responsive shielding material was designed to enable charge conversion at endo-lysosomal pH (5.5–6.5). As shown in Figure 1A, the pH-responsive shielding material was highly negatively charged at physiologic pH = 7.4 (ζ-potential value = −30 ± 2 mV, n = 3), which is crucial for the stability of the particle in the bloodstream. Next, as the pH was decreased to 5.5–6.0, the ζ-potential of the pH-responsive shielding material gradually increased and reached a value of +23 ± 2 mV at pH 5.5. In contrast, the pH-insensitive shielding material had a negative surface charge at pH 7.4–5.5 (ζ-potential value = −57 ± 2 mV at pH 7.4 and −46 ± 4 mV at pH 5.5) (Supporting Information, Figure S3).

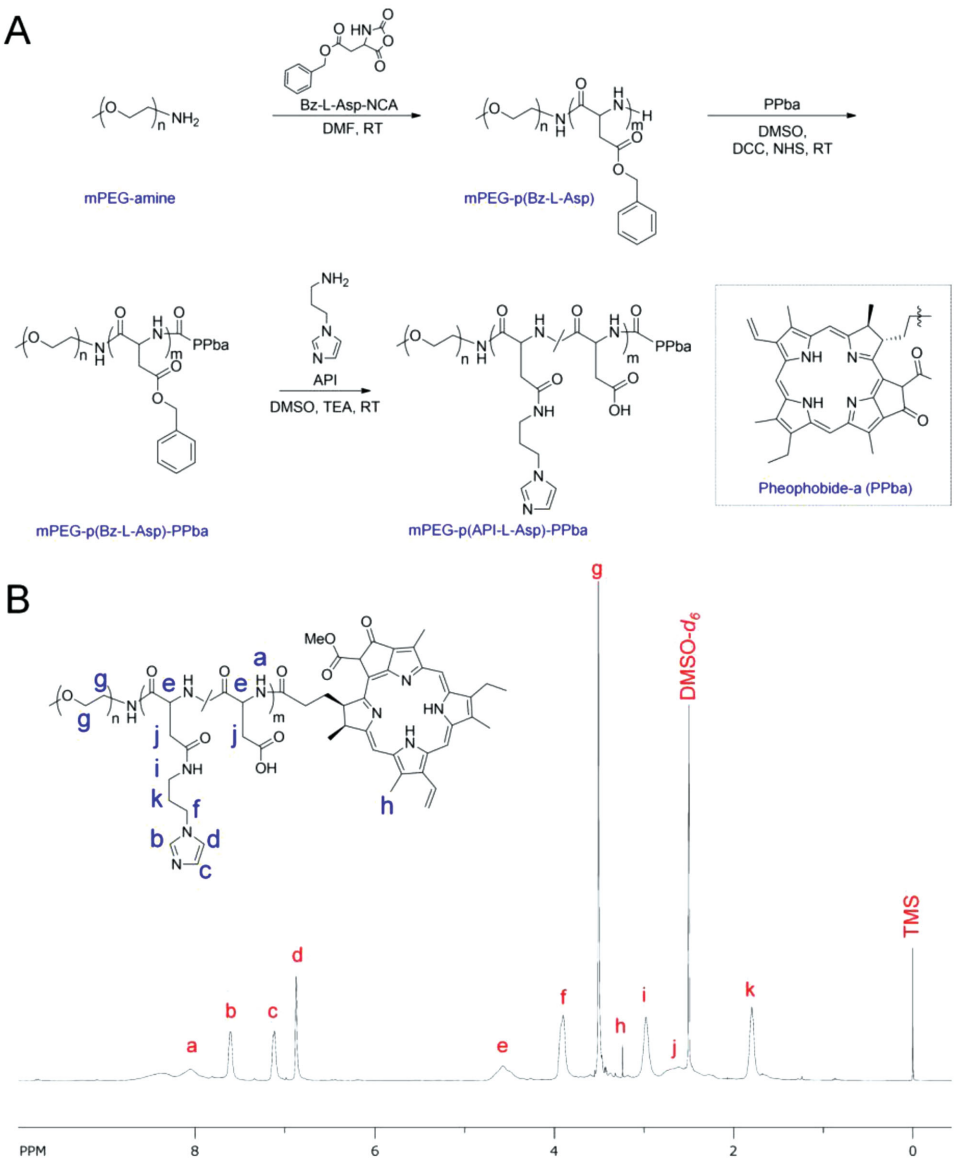

Figure 1. Chemical synthesis of pH-responsive shielding materials. A) Synthetic route and B) ^{1}H-NMR analysis (in DMSO-d_6) of pH-responsive shielding materials (mPEG-p(API-L-Asp)-PPba, $n = 45$, $m = 45$).

To formulate the pH-responsive shielding material-incorporated ternary gene complexes (pH-TCs), pDNA (GFP)/polyethylenimine (PEI, cationic polymer) complexes (nitrogen group of PEI/phosphate group of pDNA, NP ratio = 10) were first prepared as nano-sized (150 ± 10 nm) and highly positive charged (ζ-potential value = 30 ± 1 mV). Subsequently, the mPEG-p(API-Asp)-PPba was added to the pDNA/PEI complexes with various weight ratios of pH-responsive shielding materials and pDNA/PEI complexes (w/w, from 0 to 50, **Figure 2**B). The optimal formulation condition for the pH-TCs was identified by DLS. As shown in Figure 2B, the particle size of the ternary complex sharply decreased when the w/w ratio increased from 1 to 5 (from 680 ± 15 nm to 100 ± 2 nm). A further increase of the w/w ratio only slightly changed the ternary complex size. The measurement of the surface charge depending on the w/w ratio brought a detailed insight into the optimized formulation condition between mPEG-p(API-Asp)-PPba and pDNA/PEI complexes. First, at w/w ratios from 1 to 5, the ζ-potential of pH-TCs was positively charged, and it was slightly negatively charged (ζ-potential value = –6 ± 1 mV) at a w/w of 10. However, as we expected, the surface charge of the ternary complexes was significantly negative (ζ-potential value = –22 ± 1 mV) at a w/w ratio of 30, which demonstrated that stable complexes are formed between mPEG-p(API-Asp)-PPba and pDNA/PEI complexes. Furthermore, at a w/w ratio of 50, the pH-TCs have a more significantly negative charged surface (ζ-potential value = –27 ± 1 mV) and a slightly smaller size profile that has a more narrow PDI value compared with pH-TCs that have a w/w ratio of 50. Therefore, pH-TCs composed of mPEG-p(API-L-Asp)-PPba and pDNA/PEI complexes at the weight ratio of 50:1 were

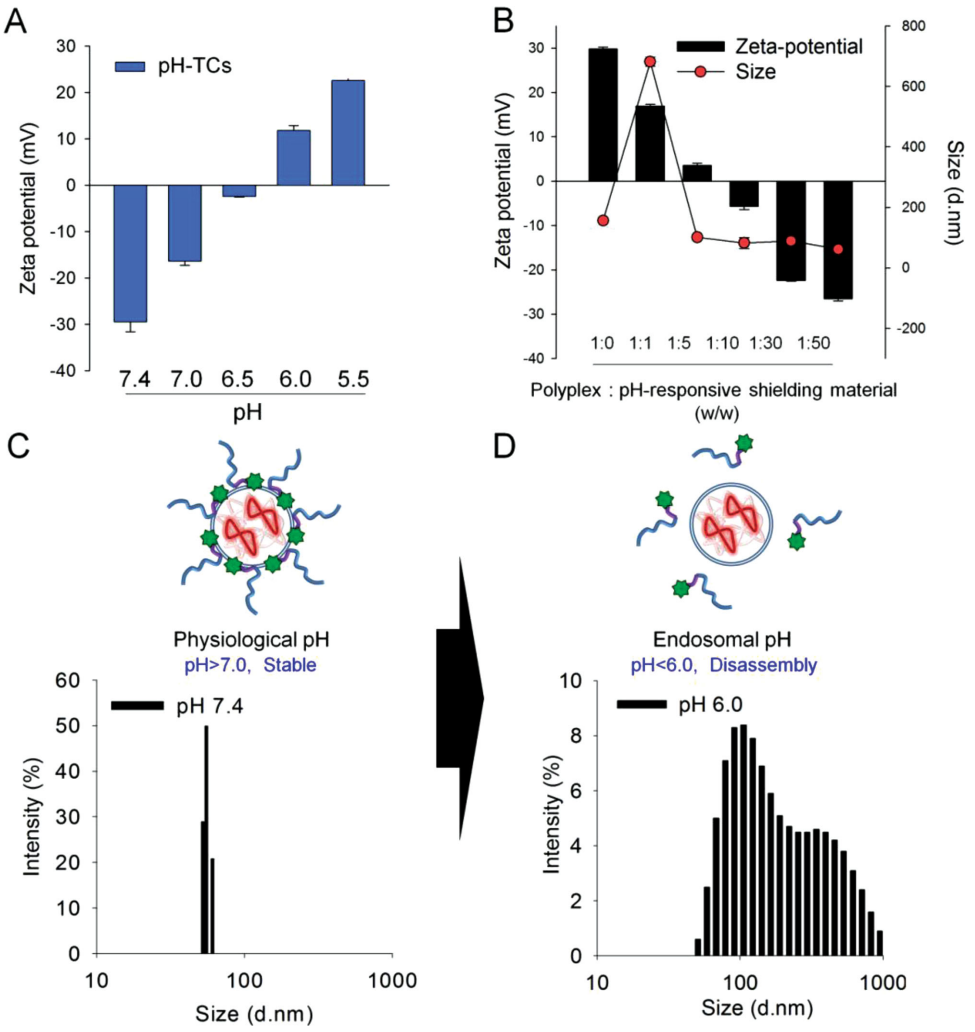

Figure 2. Characterization of pH-responsive shielding material and the change of size and surface charge of pH-TCs as a function of pH. A) Change of surface charge of pH-responsive shielding material as a function of pH ($n = 3$). B) Size and surface charge of pH-TCs depending on pH-responsive shielding material to pDNA/PEI complexes (w/w) ratio ($n = 3$). C,D) The size distribution of pH-TCs at pH 7.4 and 6.0 showing a PDI value of 0.1 and 0.6, respectively.

selected for further experimentation. Successful complexation between pH-responsive shielding and pDNA/PEI materials was further verified by a gel retardation assay (Supporting Information, Figure S4).

As mentioned above, pH-responsive shielding material was designed to enable intracellular-environment-triggered decomplexation caused by the deprotonation of imidazole groups under endo-lysosomal pH conditions for the avoidance of undesirable damage to the cargo gene by ROS generated from PS. To confirm pH-dependent decomplexation of pH-TCs, particle size distribution was measured by DLS at different pH values (Figure 2C,D). The average size of pH-TCs at pH 7.4 was found to be 64 ± 2 nm, with a narrow PDI value (Figure 2C), while that of pH-TCs at pH 6.0 was approximately 552 ± 87 nm, with a broad size distribution (PDI = 0.6), which demonstrates that ionized imidazole groups of pH-responsive shielding material repel each other via charge–charge repulsion and result in the swelling or disintegration of shielding materials from pDNA/PEI complexes. In contrast, the DLS result of pH-insensitive ternary complexes (pH-ins-TCs) was nearly similar, regardless of pH values (Supporting Information, Figure S5), indicating that the structure of those complexes was not influenced by a pH change.

2.2. In Vitro Light/pH-Selective Gene Expression by pH-TCs

To evaluate the efficiency of gene expression caused by pH-TCs, in vitro transfection experiments were conducted using the GFP gene as a reporter in K-1735 murine melanoma cells. The pH-TCs and pH-ins-TCs incorporating GFP gene were incubated with K-1735 cells in complete Eagle's minimal essential medium (EMEM) for 4 h; then, cells were irradiated with a 671 nm laser source at a power from 0 to 2.0 J cm^{-2}. The cells were then further incubated for 48 h. The level of GFP gene expression was analyzed by quantitative real-time polymerase chain reaction (real-time PCR), western blot, and confocal microscopy (**Figure 3**). The GFP expression in pH-TCs-treated

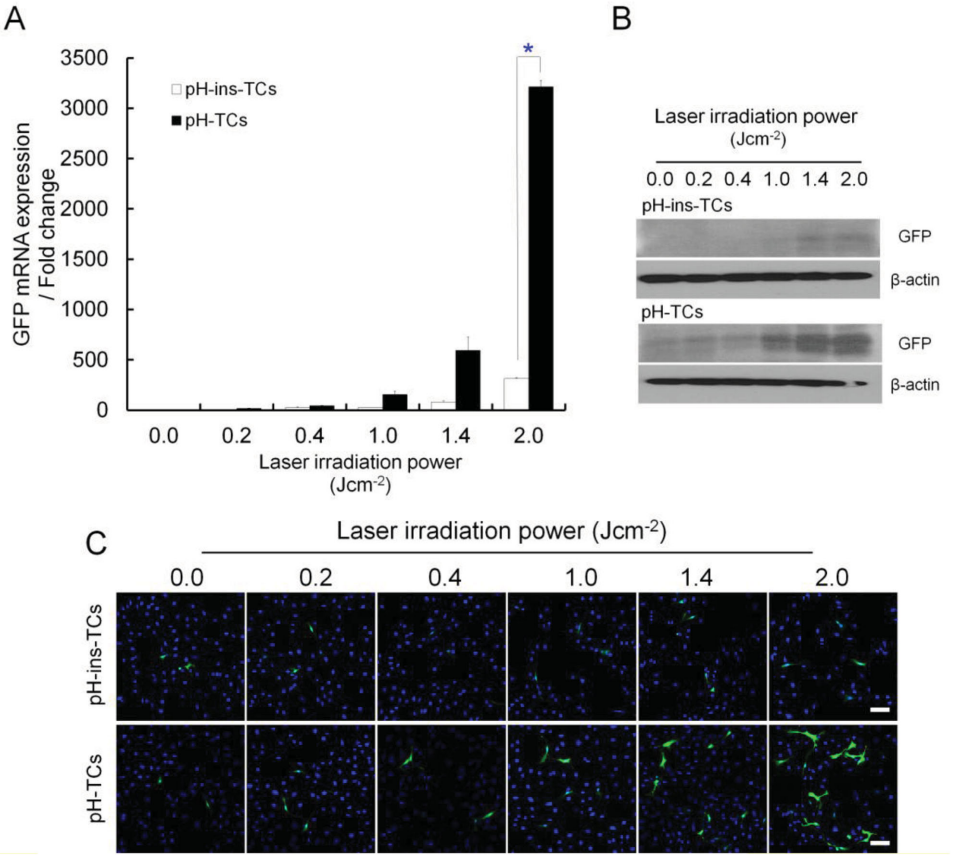

Figure 3. In vitro light/pH-selective gene expression by pH-TCs and pH-ins-TCs. The pH-TCs and pH-ins-TCs incorporating GFP gene were incubated with K-1735 cells. Subsequently, the cells were irradiated with laser power of 0.2–2.0 J cm^{-2}. A) The real-time PCR analysis of the GFP mRNA expression level depends on both laser irradiation and pH-sensitivity of shielding material. The GFP expression levels of pH-TCs and laser treated cells increased 3215- and 10-fold relative to those of pH-TCs treated cells without laser irradiation or pH-ins-TCs and laser treated cells, respectively ($n = 3$, $*P < 0.005$). B) The western blot and C) immunocytochemistry analysis of pH-TCs or pH-ins-TCs treated cells as a function of laser irradiation (scale bar: 100 μm).

group was significantly increased with increasing laser power, while that of pH-ins-TCs-treated groups only slightly increased at the strong laser irradiation power (2.0 J cm^{-2}). Notably, when a light power of 2.0 J cm^{-2} was used, pH-TCs had a greatly increased transfection efficacy, which was 10-fold more efficient than that of pH-ins TCs. This result indicates that the enhanced internalization of gene complexes by PCI-mediated endo-lysosomal disruption contributes to the transfection improvement of pH-TCs. However, the low transfection efficacy of pH-ins TCs could be attributed to plasmid damage by the neighboring activated PS mediated by the singlet oxygen.[17] Based on these results, we hypothesized that the plasmid in the pH-TCs was not affected by the singlet oxygen generated from PS because the pH-sensitive shielding material could be dissociated from the plasmid under the endo-lysosomal-pH condition.

To prove our hypothesis that pH-TCs prevent photo-oxidation of the cargo gene, pH-TCs and pH-ins-TCs were irradiated with a laser, and then, the damaged cargo DNA was analyzed by electrophoresis. As shown in Figure S6 (Supporting Information, the band intensity of DNAs extracted from pH-TCs was not decreased, regardless of laser irradiation or not, which suggests that pH-TCs could be de-shielded at endo-lysosomal pH and, subsequently, the distance between the pH-responsive shielding material and the DNA was reduced, which resulted in protection of the cargo gene from photo-oxidation. On the other hand, although the pH-ins-TCs did not induce DNA damage when it was not irradiated, the band intensity of DNAs extracted from pH-ins-TCs after laser irradiation was decreased and smeared DNA was observed. This result clearly suggests that the pH-induced dissociation property of pH-responsive shielding materials prevents photo-oxidative damage that eventually leads to successful light-triggered transfection without undesirable cargo gene damage.

2.3. Light-Triggered Endo-Lysosomal Disruption Capability of pH-TCs

As we described above, it is known that the successful escape of cargo gene complexes from the endo-lysosome, which is a digestive organelle, is a crucial key factor for improved gene delivery efficacy. Our pH-TCs were designed to (1) be de-shielded under endo-lysosomal pH conditions for safe light-triggered transfection and (2) disrupt the endo-lysosomal membrane by PS-induced local singlet oxygen generation. To verify the light-triggered endo-lysosomal disruption capability

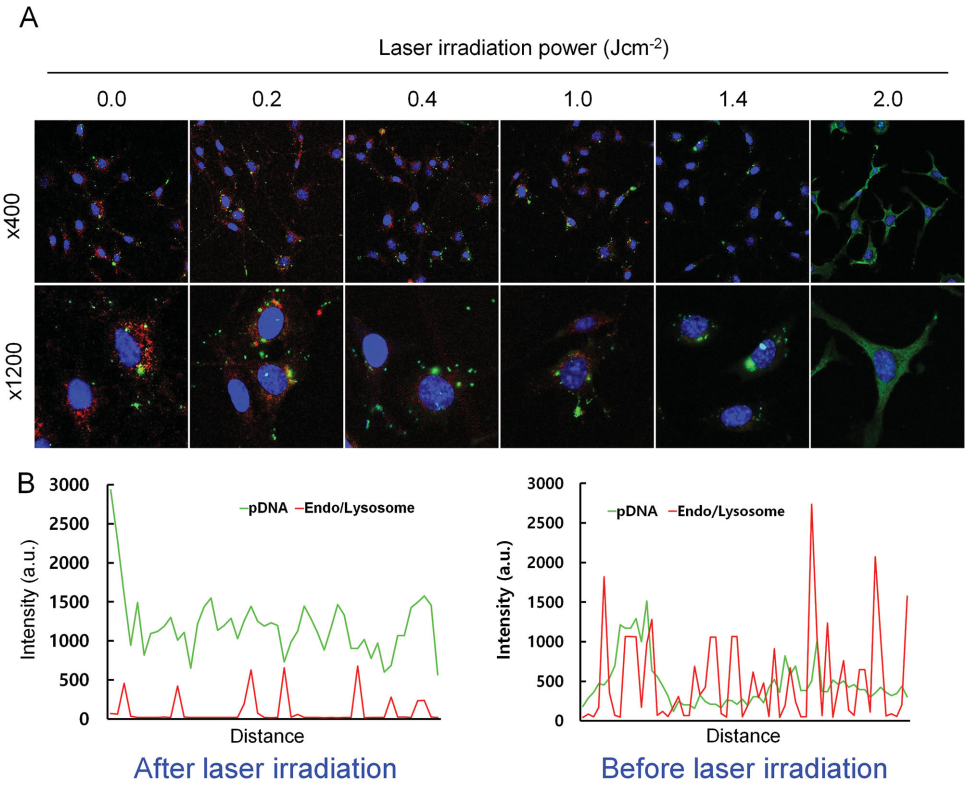

Figure 4. Light-triggered endosomal disruption capability of pH-TCs. A) The confocal microscopic analysis of light-triggered endosomal disruption and escape. The endo/lysosomal vesicles gradually disappeared and YoYo-1 intercalated genes started to leak into the cytoplasm in laser irradiated cells. (The cells were counterstained with DAPI. The green and red fluorescence indicates pDNA and endo/lysosome, respectively. Scale bar: 50 μm.) B) The co-localization histogram of pDNA and endo/lysosome. After irradiation, the fluorescence intensity of endo/lysosome decreased and was not merged with fluorescence signal of pDNA.

of pH-TCs, co-localization of genes and endo-lysosomal vesicles was observed using confocal microscopy. The signals from the YoYo-1 intercalated gene, Lysotracker Red, and DAPI are depicted with green, red, and blue, respectively. As shown in **Figure 4**A, before the laser treatment, YoYo-1 intercalated genes co-localized with endo-lysosomal vesicles, as indicated by the presence of punctate fluorescence. This pattern was quite different upon light irradiation. As cells were irradiated, endo-lysosomal vesicles gradually disappeared and YoYo-1 intercalated genes started to leak into the cytoplasm. Especially in the laser power range from 1.4 to 2.0 J cm^{-2}, the Lysotracker showed few or any punctate vesicles, and punctates of green fluorescence (YoYo-1 intercalated genes) were released from endo-lysosomal vesicles and were spread within the cytoplasm. These data clearly demonstrate that the efficient disruption of endo-lysosomal vesicles and translocation of genes from the endo-lysosomal compartment into the cytosol were conducted by light irradiation. The endo-lysosomal escape ability was further visualized by a co-localization histogram (Figure 4B). The fluorescence profiles of the endo-lysosome (red color) and YoYo-1 intercalated genes (green color) overlapped in nonirradiated cells, while after laser irradiation, the fluorescence intensity of the endo-lysosome decreased and was not merged with fluorescence signal of genes. These combined results suggest that pH-TCs accumulate in cells via endocytosis and subsequently trigger disruption of the endo-lysosomal vesicles under light irradiation and permit the endo-lysosomal escape of genes, eventually leading to an enhancement of the transfection efficiency.

2.4. In Vitro Light/pH-Selective Enhancement of p53 Gene Expression and p53-Mediated Cytotoxicity

Having proved the light-selective transfection ability of pH-TCs and the mechanism of this system, we determined the p53 delivery efficacy of light-trigged transfection and p53-mediated tumor therapeutic effect. Loss of the p53 gene is a frequent and critical event in cancer development as the p53 gene plays a key role in regulating apoptosis, cell cycle progression, and DNA repair. The nullification of p53 contributes to the survival and proliferation of tumors and an increased resistance to chemo/radiation therapy. Therefore, light-triggered delivery of p53 is a promising approach for the restoration of p53 in the cancer treatment.

For light-triggered p53 gene transfection using pH-TCs, K-1735 cells (p53 null cell, in Figure S7 (Supporting Information)), were treated with pH-TCs incorporating the p53 gene and were irradiated with a 671 nm laser at a power from 0 to 2.0 J cm^{-2}, and pH-TCs incorporating empty plasmid were used as the control. The expression of p53 was measured by quantitative real-time PCR and immunostaining. As shown

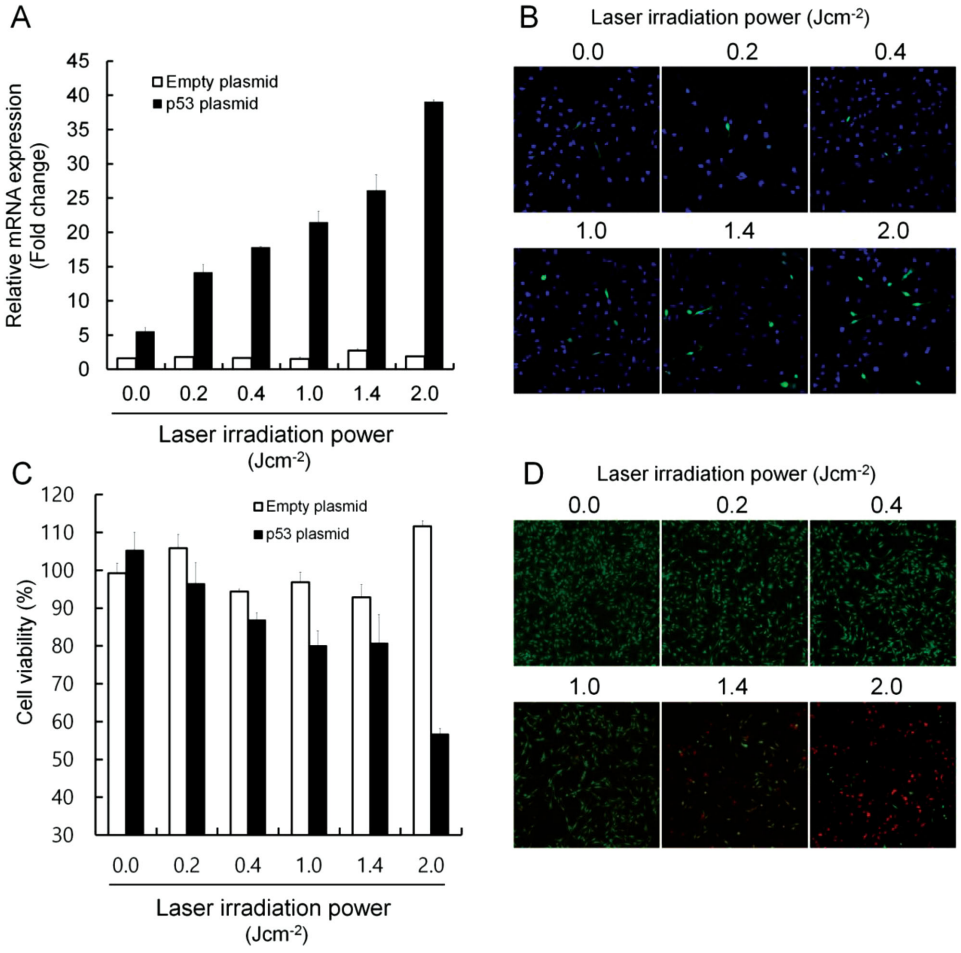

Figure 5. In vitro light/pH-selective enhancement of p53 gene expression and p53-mediated cytotoxicity. A) The real-time PCR analysis of the enhanced expression level of p53 mRNA. The p53 mRNA level of pH-TCs incorporating p53 gene treated cells was approximately increased by 7.0-fold at a laser power of 2.0 J cm^{-2}. No significant expression of p53 mRNA was observed in the cells, whether irradiated or not, treated with pH-TCs incorporating empty plasmid ($n = 3$, $^*P < 0.005$). B) Immunocytochemistry analysis of pH-TCs incorporating p53 gene or empty plasmid-treated cells as a function of laser irradiation. (The cells were counterstained with DAPI. The green fluorescence indicates p53 protein. Scale bar: 100 μm.) C) Cell counting kit-8 (CCK-8) ($n = 3$, $^*P < 0.005$) and D) live/dead analyses of the cells treated with light-triggered p53 transfection. The cytotoxicity results showed that there is a significant increase in cell death with light-triggered transfection with pH-TCs incorporating p53 gene, but not in that of pH-TCs incorporating empty plasmid.

in **Figure 5**A, the p53 mRNA levels of cells were gradually increased with increasing irradiation power. The K-1735 cells exposed to a laser power of 2.0 J cm^{-2} showed an approximately 7.0-fold increased expression of p53 mRNA compared with nonirradiated cells. On the other hand, no significant expression of p53 mRNA was observed in the cells, whether irradiated or not, treated with pH-TCs incorporating an empty plasmid, which demonstrated that p53 expression is due to the presence of the exogenous p53 gene and is not a nonspecific expression by pH-TCs or generated by singlet oxygen or laser irradiation. Additionally, these results support the light-triggered p53 gene expression ability of pH-TCs under irradiation. We also measured the in vitro irradiation power-dependent changes in the p53 protein level via immunofluorescence analysis (p53: green fluorescence, DAPI: blue). As shown in Figure 5B, abundant green fluorescence was observed in light-triggered transfected cells, which correlates with the real-time PCR results.

The corresponding cytotoxicity of the cells after light-triggered p53 transfection was analyzed by CCK-8 and the Live/Dead assay (Figure 5C,D). The quantification of cell viability showed that there is a significant increase in cell death with light-triggered transfection in pH-TCs incorporating the p53 gene. As show in Figure 5C, the cells treated with pH-TCs incorporating the p53 gene and irradiation of 2.0 J cm^{-2} had a viability of 56.7 ± 3.0%; in contrast, without laser irradiation, there is no sign of cytotoxicity (105.2 ± 14.3%). Live/dead staining results also indicated the significant cell death of the light-triggered transfected group (Figure 5D). In contrast, cells transfected with pH-TCs incorporating the control gene had no noticeable cytotoxicity at all of the tested ranges of irradiation power (from 0 to 2.0 J cm^{-2}), again supporting that the tumor cell killing effect is due to the light-triggered enhanced expression of p53 and not the photo-toxicity of PS. However, further increasing laser power caused phototoxicity, which is due to the oxidative damage of cellular components by ROS (Figure S8,

Supporting Information). This result suggested that PS requires high light doses for PDT compared to light-triggered transfection. In in vitro systems, PDT may effectively induce photo-toxicity by increasing the irradiation power. However, in 3D cultured cells and in vivo and/or clinical systems, the therapeutic outcome of PDT is limited due to the low penetration of light into deep tissue. Therefore, a combination system of PDT and light-triggered gene expression, which requires relatively low light doses, could be the best approach to treat cancer and has the potential for clinical application.

2.5. Light-Triggered Penetration and Localization of pH-TCs

Before we tested the effect of light-triggered transfection in an animal model, we assessed the tumor penetration behavior of pH-TCs by light irradiation. Unlike the in vitro situation, the actual tumor is composed of a richly well-organized extracellular matrix.[18] Therefore, even though the therapeutic effectiveness of the light-triggered transfection system is approved in vitro, the penetration/diffusion problem of nanoparticles into the deep tumor site must be overcome. In this system, we expected that the direct damage induced by the PDT effect in the dense tumor region, including extracellular matrix components, vascular cells, and tumor cells, might increase the interstitial space and reduce the volume of the extracellular matrix, thereby allowing the pH-TCs to penetrate into deeper tumor regions (Figure S9, Supporting Information).

To confirm the tumor penetration of pH-TCs, accumulation of pH-TCs was accessed in the tumor site by tracking the fluorescence of pH-TCs after laser irradiation. Mice bearing K-1735 melanoma were injected intravenously (i.v.) with pH-TCs (dose: PPba, 0.04 mg kg^{-1}). After 18 h, tumors were irradiated with a laser source (laser power, 100 J cm^{-2}), and nonirradiated mice were used as a control. After 8 h, the tumors received a second injection in the same manner as the first injection. At 24 h after the post-second injection, mice were sacrificed and an ex vivo optical image of the isolated main organs was monitored. Ex vivo imaging of isolated tumors showed the light-triggered diffusion of pH-TCs. Interestingly, as shown in **Figure 6**A, significant fluorescence signal was observed in the tumor region regardless of laser irradiation. This result indicated that pH-TC has a superior tumor-targeting capacity: the tumor targeting efficiency was approximately 17%. Furthermore, after laser treatment, the fluorescence intensity of tumors from pH-TCs was significantly increased than that of tumors from nonirradiated mice. The light-triggered enhanced accumulation of pH-TCs in tumor tissues was further verified by confocal microscopic images of tumor tissue sections (Figure 6B). In organs from irradiated mice, a weak fluorescence signal was found in the kidney and liver but not in any other organs. In contrast, signal intensities of the liver, kidney, and lung from nonirradiated mice were noticeably bright, suggesting that the particles that failed to penetrate into the tumor tissue accumulated in other organs. The fact that the tumor accumulation of pH-TCs was significantly increased in irradiated mice suggests that a partial disruption of tumor tissue by light irradiation might increase the interstitial space of the tumor; therefore, it led to the deeper tissue penetration of pH-TCs.

2.6. In Vivo Tumor Therapeutic Enhancement by Light-Triggered p53 Transfection

The data presented above indicate that a light-triggered transfection system efficiently down-regulated the p53 gene and led to the penetration of pH-TCs into deeper tumor regions. To demonstrate the therapeutic efficacy of this system in vivo, K-1735 tumor-bearing mice were injected with p53 plasmid alone or pH-TCs incorporating either an empty plasmid or the p53 plasmid on days 0, 2, and 4, and tumors were irradiated with a laser on days 1, 3, and 5. The tumor inhibition ability of each treatment was assessed by measuring the tumor size (**Figure 7**A,B). The size of the tumors treated with saline or p53 alone rapidly increased (a 46.2-fold and 22.6-fold increase, respectively, on day 7 compared to tumor size at the start of treatment). Light-triggered transfection with pH-TCs incorporating empty plasmid had a marginal tumor inhibition effect during treatment (18.6-fold increase on day 7). In contrast, we can see that there is a significant inhibition of tumor growth in mice treated pH-TCs incorporating the p53 plasmid and laser irradiation during the same period (6.8-fold increase on day 7). The histological changes of tumors after treatment were analyzed by hematoxylin and eosin (H&E) staining (Figure 7C). The tumor sections from the saline and p53-alone groups revealed hypercellularity and obvious nuclear polymorphism, and a few focal areas of cell death were observed in tumors treated with pH-TCs incorporating an empty plasmid and laser irradiation. In contrast, chromatin condensation, nucleus fragmentation, and necrotic cell death along with tissue disorganization were shown in the light-triggered p53 transfection group. Clusters of TUNEL staining-positive cells in pH-TCs incorporating p53 and irradiation-treated tumors also supported the therapeutic

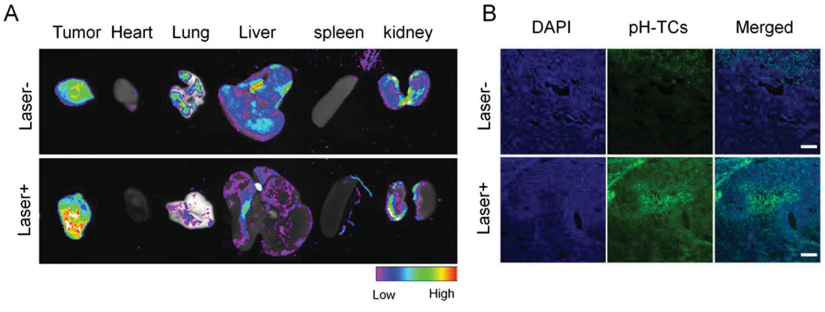

Figure 6. Light-triggered penetration and localization of pH-TCs. A) Ex vivo images of isolated main organs from pH-TCs treated mice with or without laser irradiation. The tumor of pH-TCs injected mice bearing K-1735 melanoma was irradiated with a laser. Subsequently, the tumors received a second injection of pH-TCs. In the ex vivo image, the fluorescence intensity of tumors from pH-TCs and laser treated mice was significantly higher than that of tumors from nonirradiated mice. B) Cryosections of ex vivo tumors. The sections were counterstained with DAPI. The green fluorescence indicates the fluorescence of PS incorporated in pH-TCs (scale bar: 100 μm).

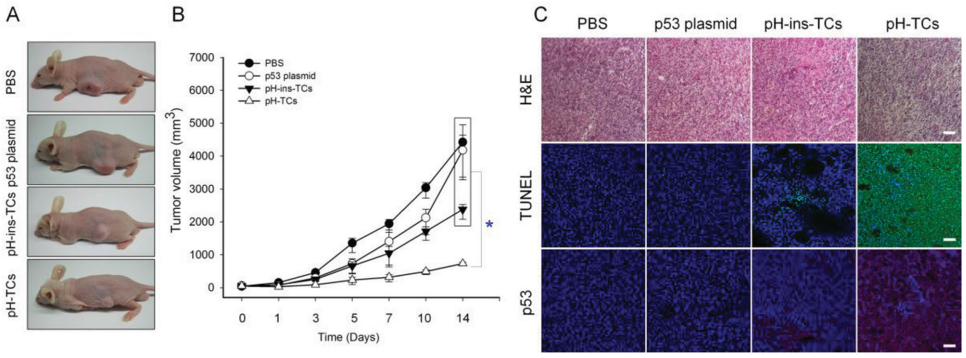

Figure 7. In vivo tumor therapeutic enhancement by light-triggered p53 transfection. A) Images of mice bearing K-1735 melanoma tumors after light-triggered p53 transfection. K-1735 tumor-bearing mice were injected with p53 plasmid alone or pH-TCs incorporating either empty plasmid or p53 plasmid on days 0, 2, and 4, and tumors were irradiated with a laser on days 1, 3, and 5. B) Change in tumor volume as a function of time after light-triggered transfection (n = 4, *P < 0.005). C) H&E (top) and TUNEL (middle) immunofluorescence (bottom, p53) staining of tumor tissue sections to assess the effectiveness of treatment. The sections were counterstained with DAPI. The green fluorescence in TUNEL staining indicates TUNEL-positive apoptotic cells. The red fluorescence in immunofluorescence staining indicates p53 proteins in tumor sections (scale bar: 100 μm).

effectiveness of this system. An immunohistochemistry analysis was conducted to confirm the expression level of p53. As shown in Figure 7C, the tumor from mice treated with pH-TCs incorporating p53 and laser irradiation showed a significantly increased expression of the p53 protein. In contrast, without the p53 gene, no significant expression of p53 was observed. In the above experiments, we demonstrated that the light-triggered p53 plasmid transfection system was able to efficiently deliver pH-TCs into a deeper tumor region. Additionally, this system efficiently released the payload from the endo-lysosomal vesicle into the cytoplasm without any damage to the plasmid from ROS due to the pH-selective de-shielding ability of pH-TCs, which resulted in the enhanced expression of the p53 gene in vitro. The in vivo tumor therapeutic result is in agreement with the in vitro results. These results indicate that the combination effect of light-triggered tumor penetration, release of payload from the endo-lysosome, and light/pH-selective p53 gene expression led to substantial inhibition of tumor growth.

3. Conclusion

In conclusion, a new light/pH-sensitive gene delivery strategy has been developed to overcome the extracellular and intracellular barriers simultaneously. In this system, pH-TCs were designed to respond to an acidic endo-lysosomal pH and light irradiation to accomplish pH/light-triggered p53 gene transfection without damage to the plasmid from ROS. With these functionalities of pH-TCs, this system induced the translocation of the payload from the endo-lysosome into the cytosol, resulting in increased gene expression under irradiation. Importantly, the pH-TCs highly accumulated in and penetrated deeper tumor regions after irradiation. This light-triggered tumor penetration/enhanced transfection provided a superior therapeutic efficacy in vivo, suggesting that this system may be used in other disease models where gene therapy could be applicable.

4. Experimental Section

Materials: β-Benzyl-L-aspartic acid (BLA), bis(trichloromethyl) carbonate (triphosgene), *N*,*N*-dimethylformamide (DMF), dimethyl sulfoxide (DMSO), dichloromethane (DCM), 1,3-dicyclohexylcarbodiimide (DCC), tetrahydrofuran (THF), triethylamine (TEA), and 1-(3-aminopropyl)imidazole (API) were purchased from Sigma-Aldrich (Sigma-Aldrich Korea, Seoul, Korea). Methoxy polyethylene glycol amine (mPEG-amine, M_n: 2 kDa) was purchased from Sunbio, Inc. (Anyang, Korea). Pheophorbide-a (PPba) was purchased from Frontier Scientific, Inc. (UT, USA). The dialysis membranes were obtained from Spectrum Laboratories Inc. (Rancho Dominguez, CA, USA). The pGFP-N1 plasmid, which expresses green fluorescent protein, was purchased from Clontech (Clontech Laboratories, USA). Expression plasmids encoding a murine p53 (PCMV6-Kan/Neo-p53) and empty vector (PCMV6-Kan/Neo) were purchased from OriGene (Rockville, MD, USA).

Synthesis of pH-Responsive Shielding Materials: Synthesis of mPEG-p(Bz-L-Asp)-PPba was performed with a slight modification from our previous method.[15] In brief, Bz-L-Asp-NCA (3 g, 12 mmol) was dissolved in a mixture of DMF (20 mL) and DCM (50 mL) at room temperature and polymerized by mPEG-NH_2(480 mg, 240 μmol). The polymer was purified by precipitation in ether (1 L) three times and then dried under vacuum. To synthesize mPEG-p(Bz-L-Asp)-PPba, PPba was conjugated to the terminal amine group of PEG-p(Bz-L-Asp) by the conventional carbodiimide reaction. mPEG-p(Bz-L-Asp) (M_n: 12 kDa, 0.2 g, 17 μmol) and a mixture of PPba (16 mg, 26 μmol), dicyclohexylcarbodiimide (8 mg, 39 μmol), and *N*-hydroxysuccinimide (5 mg, 39 μmol) were dissolved separately in DMF (10 mL), and the solutions were stirred thoroughly for 3 h prior to the condensation reaction. The two reactant solutions were then mixed and stirred at room temperature. After 24 h, the reaction mixture was purified by precipitation in ether (0.2 L) three times and then dried under vacuum. Finally, mPEG-p(API-L-Asp)-PPba was synthesized via aminolysis of mPEG-p(Bz-L-Asp)-PPba with API. mPEG-p(Bz-L-Asp)-PPba (0.2 g, 16 μmol) was dissolved in DMF (5 mL), followed by reaction with API (80 mg, 640 μmol) and TEA (16 mg, 160 μmol) under nitrogen atmosphere at room temperature for 12 h.

Size and ζ-Potential Measurements of pH-Responsive Shielding Materials at Different pHs: The size and ζ-potential of the pH-responsive shielding material and pH-responsive shielding material was measured using a DLS (Zetasizer Nano ZS, Malvern Instruments, Malvern, UK), while the pH of the solution gradually decreased from 7.4 to 5.5 by adding a 0.1 N HCl solution.

Preparation and Characterization of pH-TCs: The pH-TCs were prepared by mixing mPEG-p(API-L-Asp)-PPba with a positively charged

PEI/plasmid complex. In brief, 2 μg of PEI and 2 μg of plasmid (pGFP-N1 or PCMV6-Kan/Neo or PCMV6-Kan/Neo-p53) were dissolved in 50 μL of serum-free culture medium and incubated for 10 min. Subsequently, the mPEG-p(API-L-Asp)-PPba solution was added to pDNA/PEI complexes with various mPEG-p(API-L-Asp)-PPba to pDNA/PEI complexes (w/w), ranging from 0 to 50, and was incubated for 15 min. The size and ζ-potential of the pH-TCs were determined by DLS (Zetasizer Nano ZS, Malvern Instruments, Malvern, UK).

Cell Culture: A mouse melanoma cell line K-1735 was obtained from the Korean Cell Line Bank (KCLB No. 80013). Eagle's minimal essential medium (EMEM) was obtained from American Type Culture Collection (Manassas, VA, USA). K-1735 cells were maintained at 37 °C in a 5% CO_2 atmosphere in EMEM supplemented with 10% FBS, 100 units mL^{-1} of penicillin, and 100 μg mL^{-1} of streptomycin.

Light-Triggered Transfection: For the in vitro light-triggered transfection, K-1735 cells were seeded into 35 mm^2 cell culture dishes at 2.5×10^5 cells per dish and cultured for 24 h. The cells were treated with pH-TCs incorporating a GFP or p53 plasmid or control vector and pH-ins-TCs incorporating a GPF plasmid for 4 h. Subsequently, cells were irradiated using a 671 nm laser source with power of 0.2, 0.4, 1.0, 1.4, and 2.0 J cm^{-2}. After further incubation for 48 h, the cellular levels of GFP or p53 mRNA and protein were assessed using qRT-PCR, western blot, confocal microscopic image, and immunocytochemistry.

Western Blot Analysis: To measure the GFP protein expression level by light-triggered transfection, western blot analysis was performed. K-1735 cells were transfected as mentioned above. Forty-eight hours post-transfection, the cells were collected and lysed using RIPA buffer (Pierce, Rockford, IL, USA) containing a protease inhibitor cocktail (Roche, Germany). Thirty micrograms of total protein was separated on a 12% SDS-PAGE gel and transferred onto polyvinylidene difluoride (PVDF) membranes. The membrane was blocked in 5% skim milk and then incubated with an anti-GFP antibody (Clontech, USA). The membranes were incubated with an anti-β-actin antibody (Santa Cruz Biotech, Santa Cruz, CA) as an internal standard for protein loading. Subsequently, a horseradish peroxidase (HRP)-conjugated secondary antibody (Santa Cruz Biotechnology, Santa Cruz, CA, USA) was used to amplify the signal. Protein signals were detected using a chemiluminescence system (New Life Science Products, Boston, MA, USA).

Real-Time PCR: The GFP and p53 mRNA level due to light-triggered transfection was quantitatively determined by real-time PCR analysis. Total RNA from the cells was isolated using the Trizol reagent (Invitrogen, Carlsbad, CA, USA). Five-hundred nanograms of total RNA was used for first-strand cDNA synthesis. Real-time PCR analysis was performed using 1 μg of cDNA and SYBRGreen PCR Master Mix (Applied Biosystems, Warrington, UK) in a 7500 Fast Real-Time PCR System (Applied Biosystems, Warrington, UK). GAPDH was used as a reference gene. The specific forward and reverse primer sequences were as follows: GFP (F); 5′-TGAACCGCTCGAGCTGAAGGG-3′, GFP(R); 5′-TCCAGCAGGACCATGTGATCGC-3′, p53 (F); 5′-AGAGAC-CGCCGTACAGAAGA-3′, p53(R); 5′-CTGTAGCATGGGCATCCTTT-3′. PCR parameters were as follows: one cycle of 2 min at 95 °C, followed by 30 s at 95 °C, 30 s at 55.6 °C, and 60 s at 72 °C for 40 cycles.

Confocal Microscopy Imaging of Light-Triggered Endo-Lysosomal Disruption: K-1735 cells were seeded into 35 mm^2 cell culture dishes at 2.5×10^5 cells per dish and treated with pH-TCs incorporating YoYo-1 intercalated plasmid (with a pDNA to YoYo-1 weight ratio at 10:1). After 4 h, cells were irradiated using a 671 nm laser with power of 0.2, 0.4, 1.0, 1.4, and 2.0 J cm^{-2}. Subsequently, the cells were further incubated with Lysotracker Red (Invitrogen, Carlsbad, CA, USA) for 2 h. The cells were mounted with a mounting solution containing DAPI and visualized using a confocal laser scanning microscope (Zeiss LSM 710Meta, Oberkochen, Germany). Images were analyzed using LSM Image Browser software (Zeiss).

Immunohistochemistry: The cells were fixed in 4% paraformaldehyde and blocked with 5% BSA for 30 min. Then, cells were incubated with an anti-p53 antibody (Cell Signaling Technology, Beverly, MA, USA) at 4 °C overnight. Then, the cells were incubated for 60 min at ambient temperature with a DyLight 488-conjugated secondary antibody for further confocal laser scanning microscope analysis.

In Vitro Cytotoxicity: Cell viability was measured by the cell counting kit-8 (CCK-8) and Live/Dead assays. For the CCK-8 assay, the cells were incubated with 100 μL of CCK-8 solution. After 4 h, absorbance intensity was measured at 450 nm using a microplate reader (Bio-Tek, VT, USA). For the Live/Dead assay, the cells were incubated with 2×10^{-3} M calcein AM and 4×10^{-3} M EthD-1 (Invitrogen, Carlsbad, CA, USA). Images of live and dead cells were obtained using a fluorescence microscope (Carl Zeiss Axio Imager M2, Oberkochen, Germany).

In Vivo Studies: All of the in vivo studies conformed to the Guide for the Care and Use of Laboratory Animals published by the National Institutes of Health, USA (NIH publication no. 85-23, 1985, revised 1996), and mice were maintained under the guidelines of an approved protocol from the Institutional Animal Care and Use Committee (IACUC) of the Catholic University of Korea (Republic of Korea).

Ex Vivo Image of Light-Triggered Penetration of pH-TCs: For the subcutaneous melanoma tumor model, 6 week old male nude mice were inoculated with K-1735 cells (1×10^6 cells/mice). The total number of mice for this experiment was six ($n = 3$ mice per group). Fifteen days after inoculating the tumor cells, the mice received an i.v. injection with the pH-TCs (dose: PPba, 0.04 mg kg^{-1}). After 18 h, tumors were exposed to the laser (laser power of 100 J cm^{-2}), and nonirradiated mice were used as control. After 8 h, mice received a second injection in the same manner as the first injection. At 24 h after the post-second injection, mice were sacrificed and isolated main organs were imaged with the KODAK image station (Image Station 4000 MM; Kodak, New Haven, CT). The fluorescence level of each organ was analyzed by Image J software (National Institutes of Health, Maryland, USA). Substantially, the isolated tumors were fixed in 10% neutral buffered formalin and frozen sectioned into 5 μm thick slices. The sections were counterstained with DAPI and observed with a confocal laser scanning microscopy.

In Vivo Light-Triggered Therapy: The in vivo response to the light-triggered transfection of pH-TCs incorporating p53 gene was assessed by measuring the tumor size and histological analysis. The total number of mice for this experiment was 16 ($n = 4$ mice per group). Mice were inoculated with K-1735 cells. After 10 d, mice received a systemic injection with either PBS or p53 plasmid alone or with pH-TCs incorporating either empty plasmid or p53 plasmid on days 0, 2, and 4, and tumors were irradiated with a laser on days 1, 3, and 5. The tumor size and body weight were measured. The tumor volume, V, was calculated using the formula $V = a^2 \times b/2$, where a is width, b is length, and $a \leqq b$. For histological analysis, the tumors were harvested and frozen sectioned into 5 μm thick slices. The tumor sections were stained with hematoxylin and eosin according to standard protocols. For the terminal deoxynucleotidyl transferase dUTP nick end labeling (TUNEL) assay, the sections were incubated with 0.1% Triton X-100. Subsequently, tumor sections were incubated with the TUNEL reaction mixture for 1 h at 37 °C. The stained sections were mounted with mounting medium containing DAPI and observed by confocal laser scanning microscopy. For fluorescent Immunohistochemistry (IHC) staining, the tumor sections were incubated in a blocking solution for 30 min. Then, the sections were stained with anti-p53 antibody at 4 °C overnight and detected with DyLight 488-conjugated secondary antibodies (Abcam, Cambridge, MA, USA). The stained tumor section was analyzed by confocal laser scanning microscopy.

Statistical Analysis: The results were expressed as mean ± standard deviation (SD). Differences between the values were assessed using Student's t-test.

Supporting Information

Supporting Information is available from the Wiley Online Library or from the author.

Acknowledgements

S.P. and W.P. contributed equally to this work. This work was supported by the Strategic Research through the National Research Foundation of Korea (NRF) grant funded by the Korea government (MSIP) (No. 2011-0028726).

Received: February 23, 2015
Revised: April 7, 2015
Published online: May 5, 2015

[1] a) T. Niidome, L. Huang, *Gene Ther.* **2002**, *9*, 1647; b) R. C. Mulligan, *Science* **1993**, *260*, 926; c) K. J. Fisher, K. Jooss, J. Alston, Y. Yang, S. E. Haecker, K. High, R. Pathak, S. E. Raper, J. M. Wilson, *Nat. Med.* **1997**, *3*, 306; d) I. M. Verma, N. Somia, *Nature* **1997**, *389*, 239.
[2] H. Li, S. S. Yu, M. Miteva, C. E. Nelson, T. Werfel, T. D. Giorgio, C. L. Duvall, *Adv. Funct. Mater.* **2013**, *23*, 3040.
[3] N. Wiradharma, M. Khan, Y. W. Tong, S. Wang, Y. Y. Yang, *Adv. Funct. Mater.* **2008**, *18*, 943.
[4] S. Lee, H. Koo, J. H. Na, K. E. Lee, S. Y. Jeong, K. Choi, S. H. Kim, I. C. Kwon, K. Kim, *ACS Nano* **2014**, *8*, 4257.
[5] W. Park, K. Na, *Wiley Interdiscip. Rev. Nanomed. Nanobiotechnol.* **2015**, doi: 10.1002/wnan.1325.
[6] a) S. Febvay, D. M. Marini, A. M. Belcher, D. E. Clapham, *Nano Lett.* **2010**, *10*, 2211; b) T. Nomoto, S. Fukushima, M. Kumagai, K. Machitani, Y. Matsumoto, M. Oba, K. Miyata, K. Osada, N. Nishiyama, K. Kataoka, *Nat. Commun.* **2014**, *5*, 3545; c) C.-S. Lee, W. Park, S.-J. Park, K. Na, *Biomaterials* **2013**, *34*, 9227; d) M. K. G. Jayakumar, A. Bansal, K. Huang, R. Yao, B. N. Li, Y. Zhang, *ACS Nano* **2014**, *8*, 4848.
[7] a) J. A. Mindell, *Annu. Rev. Physiol.* **2012**, *74*, 69; b) T. F. Martens, K. Remaut, J. Demeester, S. C. De Smedt, K. Braeckmans, *Nano Today* **2014**, *9*, 344.
[8] a) C. Wong, T. Stylianopoulos, J. Cui, J. Martin, V. P. Chauhan, W. Jiang, Z. Popović, R. K. Jain, M. G. Bawendi, D. Fukumura, *Proc. Natl. Acad. Sci. USA* **2011**, *108*, 2426; b) R. Tong, H. D. Hemmati, R. Langer, D. S. Kohane, *J. Am. Chem. Soc.* **2012**, *134*, 8848.
[9] a) A. I. Minchinton, I. F. Tannock, *Nat. Rev. Cancer* **2006**, *6*, 583; b) R. Kalluri, M. Zeisberg, *Nat. Rev. Cancer* **2006**, *6*, 392.
[10] a) K. Berg, P. K. Selbo, L. Prasmickaite, T. E. Tjelle, K. Sandvig, J. Moan, G. Gaudernack, Ø. Fodstad, S. Kjølsrud, H. Anholt, *Cancer Res.* **1999**, *59*, 1180; b) H.-L. Lu, W.-J. Syu, N. Nishiyama, K. Kataoka, P.-S. Lai, *J. Controlled Release* **2011**, *155*, 458; c) N. Nishiyama, A. Iriyama, W.-D. Jang, K. Miyata, K. Itaka, Y. Inoue, H. Takahashi, Y. Yanagi, Y. Tamaki, H. Koyama, *Nat. Mater.* **2005**, *4*, 934; d) K. Han, Q. Lei, H. Z. Jia, S. B. Wang, W. N. Yin, W. H. Chen, S. X. Cheng, X. Z. Zhang, *Adv. Funct. Mater.* **2015**, *25*, 1248; e) K. Raemdonck, B. Naeye, K. Buyens, R. E. Vandenbroucke, A. Høgset, J. Demeester, S. C. De Smedt, *Adv. Funct. Mater.* **2009**, *19*, 1406.
[11] S.-J. Park, W. Park, K. Na, *Biomaterials* **2013**, *34*, 8991.
[12] P. K. Selbo, A. Weyergang, A. Høgset, O.-J. Norum, M. B. Berstad, M. Vikdal, K. Berg, *J. Controlled Release* **2010**, *148*, 2.
[13] a) S. W. Lowe, S. Bodis, A. McClatchey, L. Remington, H. E. Ruley, D. E. Fisher, D. E. Housman, T. Jacks, *Science* **1994**, *266*, 807; b) P. G. Komarov, E. A. Komarova, R. V. Kondratov, K. Christov-Tselkov, J. S. Coon, M. V. Chernov, A. V. Gudkov, *Science* **1999**, *285*, 1733.
[14] D. Ling, W. Park, S.-J. Park, Y. Lu, K. S. Kim, M. J. Hackett, B. H. Kim, H. Yim, Y. S. Jeon, K. Na, *J. Am. Chem. Soc.* **2014**, *136*, 5647.
[15] S. Jeong, W. Park, C. S. Lee, K. Na, *Macromol. Biosci.* **2014**, *14*, 1688.
[16] M. Nakanishi, J.-S. Park, W.-D. Jang, M. Oba, K. Kataoka, *React. Funct. Polym.* **2007**, *67*, 1361.
[17] H. Wiseman, B. Halliwell, *Biochem. J.* **1996**, *313*, 17.
[18] O. Trédan, C. M. Galmarini, K. Patel, I. F. Tannock, *J. Natl. Cancer Inst.* **2007**, *99*, 1441.